Project Number: [956004]
Project Acronym: [BioTrib]
Project title: [**Advanced Research Training for the Biotribology of Natural and Artificial Joints in the 21st Century**]

Fissure propagation properties of fibrous membranes

Deliverable D5.3

Month Due: PM21

Month Delivered: PM22

Project coordinator name	Prof. Richard M Hall
Project coordinator organisation name	UNIVLEEDS
Report prepared by	Alessio Amicone Prof. Dr. Stephen J. Ferguson ETH Zürich

Dissemination Level of Report

PU	Public	
PP	Restricted to other program participants (including the Commission Services)	
RE	Restricted to a group specified by the consortium (including the Commission Services)	
CO	Confidential, only for members of the consortium (including the Commission Services)	X

The BioTrib ETN project has received funding from the European Union's Horizon 2020 research and innovation programme under grant agreement No. 956004.

Contents

Executive Summary

Today, osteoarthritis (OA) affects an estimated 250 million adults around the world [1] and is the most common degenerative joint disease, a major cause of pain and disability, and a source of high societal cost [2]. The disease compromises the structural and functional integrity of articular cartilage – the thick, load-bearing tissue lining the ends of long bones – as well as the adjacent bone and other joint tissues [3]. These biological changes cause pain and limited mobility, which profoundly impact a person's everyday life. OA thereby leads to social, economic, and societal burdens, which are further compounded by the health challenges associated with increasing life expectancy and prevalence of obesity in our global population [4].

While OA is often described as a condition resulting from the wear-and-tear on joints, the pathophysiology of this condition is much more complex, and the detailed mechanisms underpinning OA initiation and progression remain poorly characterized [4]. Several studies have emphasized the importance of mechanical factors in the destructive cascade of this disease, and thus the role of biomechanics in the development and progression of OA is becoming integral to advancing our understanding of this devastating disease [4].

The aim of this project is to advance the understanding of tissue biomechanics, specifically the onset of failure in cartilage and in cartilaginous tissues, by combining experimental tests with computer simulations of the fracture mechanism of fibrous materials. The results will be used to improve the performance of both natural and artificial joints for OA patients, with a focus on biotribology, which includes friction, lubrication, and wear in these interventions.

The objectives of this project will be accomplished through the following steps:

1. Develop a fiber-reinforced finite element (FE) model of cartilage
2. Produce electrospun and melt-electrowritten grafts mimicking the fibrous membrane of cartilage
3. Characterize fissure initiation and propagation properties of multiscale fibrous membranes
4. Identify articulating conditions that may cause damage
5. Incorporate experimental data into the FE model to facilitate model improvement

The scientific deliverables in this project will be broadly applicable in the field of soft tissue engineering, where a better understanding of the fibrillation initiation and growth could help to stop or reduce the OA relapse cycle. Furthermore, the project will contribute new finite element models to examine the causative pathways by which the local mechanical environment of damaged cartilage causes cartilage degeneration. Lastly, as an alternative approach to electrospinning, we are trying to develop new methods for melt electrowriting, with the aim of producing hierarchical nano- and microfibrous tissue scaffolds with integrated reinforcing elements.

This report includes:

- Methods for the generation of fibrous membranes by electrospinning technique
- Tensile tests to measure the mechanical properties of engineered cartilage tissues
- Tensile crack propagation tests presenting a first characterization of fissure initiation and propagation properties of multiscale fibrous membranes
- First attempt of building a fiber-reinforced model for articular cartilage

Introduction

Osteoarthritis (OA) and the articular cartilage

Osteoarthritis (OA) is a prevalent and incapacitating ailment that places a significant and rising burden on health care systems, the affected individuals, and broader societal expenses. Estimates indicate that 528 million individuals [5] are currently afflicted due to the impacts of aging and rising obesity rates in the world's population, together with an increase in the number of joint injuries [1]. OA is viewed as a whole-joint illness with a multifactorial etiology that includes increased mechanical stress, ligament sprains, cartilage breakdown, subchondral bone alterations, and muscle impairments [4]. The causes of OA are largely unknown, and the risk of developing OA depends on a number of genetic and environmental causes [6]. OA is a common illness in the elderly, although younger people might develop mechanically induced OA as a result of an injury or chronic overloading of the tissue [7].

Instead of being solely a passive degenerative disease or so-called wear-and-tear disease as is typically defined, the disease is an active dynamic modification resulting from an imbalance between the repair and destruction of joint tissues [1]. OA occurs when the cartilage, a thin layer of tough, smooth, and slippery tissue in between the bones in a joint, gradually erodes. As result, subchondral sclerosis and cysts occur, followed by synovial inflammation, and marginal osteophyte formation. There is currently no "restitutio ad integrum", or medical cure, for OA. OA and biomechanics are inescapably linked together. However, the contribution of biomechanical factors to etiology, pathogenesis, and to disease progression requires further research in order to reduce the enormous socioeconomic and personal impact of this disease [4].

Articular cartilage is an avascular, alymphatic, and aneural soft tissue that transmits loads to the subchondral bone beneath by reducing friction between articulating bone surfaces [8]. It is made up of a sparse distribution of chondrocytes, which are highly specialized cells surrounded by a dense extracellular matrix (ECM). The extracellular matrix (ECM) is predominantly composed of water, proteoglycans (with small amounts of other proteins), a collagen network, and ions (mostly Na^+ and Cl^-) [9]. These elements help maintain the water balance, which is essential to maintaining the mechanical properties of articular cartilage [8]. Additionally, the compressive strength of cartilage is provided by water and proteoglycans, and its resistance to tensile stresses is aided by collagen fibrils [8]. As a result of the association between joint inactivity and cartilage degradation, frequent joint motion and the application of dynamic weight are crucial for maintaining healthy cartilage. However, high mechanical loading increases the risk of OA pathogenesis and development [10].

Because of its depth-dependent structural and compositional distribution, articular cartilage is a heterogeneous and anisotropic material. The Superficial (tangential) zone, Middle (transitional) zone, Deep Zone, and Calcified Zones are the four unique zones that make up articular cartilage. In each of these zones, the cells differ in size, shape, and metabolic activity. The superficial zone contains the most collagen and water, with the middle (transitional) and deep zones having lower concentrations of both. The pattern for proteoglycan content is the opposite [8]. Due to the parallel orientation of the collagen fibers with respect to the articular surface, the superficial zone is known to be more resistant to shear stress and wear than the deeper layers [11].

Human cartilage undergoes continuous remodeling throughout life as chondrocytes swap out broken-down macromolecules in the matrix for freshly created ones. This process can take up to two decades. However, due to its poor vascularity and glacial metabolic activity, articular cartilage has a poor ability to heal even a little lesion and to restore mechanical function [9]. So, once the damage has occurred, a feedback cascade of inflammation starts to take hold. If this cascade is allowed to continue, it will eventually cause a pathological change in the gene expression patterns of the chondrocytes, which will reduce their ability to produce ECM and increase the release of enzymes that break down the matrix, ultimately resulting in the destruction of the affected joint [9].

Due to its distinctive and intricate structure, articular cartilage is challenging to treat and mend [8]. Most of the common procedures for treating OA can reduce discomfort, but they do not always result in full healing or provide a long-term solution due to inadequate mechanical function of the repaired tissue. Most recently,

scaffold-free tissue engineering techniques are considered the most promising route to creating viable articular cartilage grafts with biochemical and biomechanical properties within the range of native articular cartilage [12].

Engineered grafts and Electrospinning

Currently, regenerative medicine strategies offer a promising solution for the treatment of articular cartilage defects and potentially localized early OA. Such strategies rely on the development of materials to restore some aspects of cartilage [13]. Electrospinning and melt electrowriting (MEW) are techniques that can produce fibrous structures in the nanoscale and microscale range respectively. Due to its ability to closely resemble the scale and morphology of the extracellular matrix, electrospun and more recently melt electrowritten poly(-caprolactone) (PCL) is frequently employed as a substrate for tissue engineering (TE). Furthermore, the slow degradation of PCL provides suitable mechanical stability that allows an implant to withstand physiological levels of strain [14]. The general mechanical competence and cell compatibility of such materials for use in the reconstruction of cardiovascular, cartilage, and intervertebral disc tissues have been demonstrated.

During the electrospinning process, a polymer solution is ejected from a needle in a liquid state. Under the influence of an electric field, the polymer solution is accelerated away from the needle and toward a grounded collector, producing overlying patterns of fibers with diameters in the nano- to micrometer range (Figure 1). The thin electrospun fibers range from a few hundred nanometers to a few micrometers and are suitable candidates to mimic the structure of the natural extracellular matrix (ECM) as they can stimulate cell ingrowth and proliferation [15].

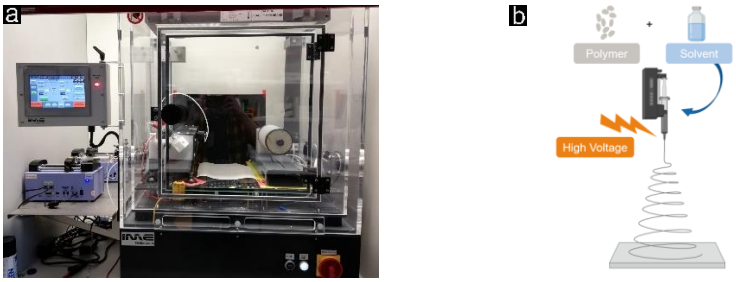

Figure 1: a) Electrospinning device. b) Electrospinning mechanism illustration.

Mechanical testing of cartilage tissue engineering

Compression, shear, friction, and tension are only a few of the diverse loading conditions to which healthy articular cartilage is exposed [16]. Injury and degeneration of articular cartilage involves a number of articular cartilage defects [17]. The joint's ability to support loads will gradually deteriorate as the number and magnitude of these defects or cracks grow. Additionally, further overload may possibly cause significant joint function deterioration or osteoarthritis. Nevertheless, the fracture behavior of articular cartilage is inextricably linked to its structure. Failure properties must be evaluated by fracture toughness techniques. There are three main fracture loading modes used in traditional fracture mechanics. Since tensile stresses are the main form of crack opening and often the most demanding criteria for material evaluation, this mode of fracture loading has been utilized most frequently for cartilage. However, it is crucial to remember that fracture mechanics techniques were initially created to assess linear elastic materials. Since articular cartilage tissue is viscoelastic, anisotropic, and made up of many layers, crack extension can vary in amplitude and mode, even with consistent loading methods, making it challenging to obtain consistent and clear fracture toughness measurements [11]. Because of the complexity of the mechanical behavior of soft collagenous tissues (SCT), it is difficult to comprehend and anticipate failure at their faults. This is also because of the difficulties associated with the variabilities observed in corresponding mechanical experiments [18].

In order to avoid cartilage damage and cure early osteoarthritis, it is crucial to study the mechanical properties of cracked cartilage [19]. Furthermore, with regards to regenerative medicine strategies, to quantify the mechanical function of the repaired or treated tissue and to ensure that these structures mimic the structure, composition, and mechanical behavior of the native tissues, evaluation of the physical properties of both the

intact and damaged membranes is essential [16]. In that way, it will be possible to understand how to best identify fracture mechanics methods most suitable for evaluating both artificial membranes and cartilage.

Fiber-reinforced modeling for articular cartilage and synthetic membranes

Understanding the various mechanisms and their interactions behind the onset and progression of mechanically induced OA is crucial to elucidate their role and to optimize treatment methods [7]. Using *in vivo* imaging techniques (MRI or CECT or *in vitro* techniques), changes in cartilage composition and structure can be detected. These imaging methods cannot, however, measure the mechanical properties of cartilage that are essential to the complex mechanical function of the joint. Furthermore, these studies face several limitations in evaluating the interactive roles of collagen disorganization and degradation in OA onset and progression [7]. Instead, it is necessary to forecast the mechanical performance of cartilage and other tissues during joint stress using computer modeling in conjunction with an imaging approach [20]. Recent advances in *in silico* approaches offer a singular integrated platform for examining the causative pathways by which the local mechanical environment of damaged cartilage causes cartilage degeneration. *In silico* models provide a unique platform to incorporate insights from *in vivo* and *in vitro* experiments. These models allow a deeper comprehension of the local mechanical environment in cartilage tissue under injurious stress, around structural defects, and its role in cartilage destruction. Several in silico models were introduced in literature in order to achieve this [7].

Despite the fact that these studies shed light on the local degenerative changes that occur in cartilage tissue, they are unable to predict alterations in the composition of cartilage constituents and their roles in various degeneration pathways or their interconnections. Furthermore, current cartilage degeneration algorithms lack biofidelty because they cannot account for the experimentally observed effect of fibril disorganization in combination with other degenerative mechanisms [21]. Having some improvements in that direction could make it easier to describe how joint loads affect tissues and cells, look into potential tissue failure locations, and predict how fiber-reinforced tissues will adapt to loading in healthy and unhealthy joints [20].

Deliverable Description

In this project, we aim to evaluate the mechanical properties of intact and notched electrospun membranes, at both the material and structural levels. A quick explanation of how to manufacture these membranes will be shown. The mechanical method used to study the properties of these membranes is also explained. A first attempt to build a poro-viscoelastic FE model of fiber-reinforced cartilage will be shown.

Deliverable Report

1. Materials and methods

1.1 Material preparation

Electrospun scaffolds were made from poly(ε-capro-lactone) (PCL), a slowly degrading, biocompatible polymer with well-understood properties and prior application in tissue engineering.

Starting from work recently developed in collaboration with ESR1 Elisa Bissacco [22], we electrospun 4 different structure types with random (4-hour spin) and aligned orientation of the fibers (spin of 4, 6 and 8 hours). Therefore, to adjust fiber alignment, the electrospinning collector rotation velocity was increased (1200 rpm) and conduction gaps on the collector were introduced through a Kapton insulating tape (12 mm).

In both fiber alignment conditions, the electrospinning device (EC-CLI, IME) was used to fabricate PCL electrospun matrices, consisting of nanofibers between 350 nm and 850 nm in diameter. PCL (Mw 80.000) polymer pellets were dissolved in CH3OH:CHCl3 + 0.04 % NaCl overnight at room temperature to create 11 % w/v concentration solution. The electrospinning flow rate was set to 1.62 ml/h, and a 20 cm working distance was used. A 10 ml glass syringe with 20G needle was used to spin the solution onto the rotating collector. Temperature and relative humidity around the device were controlled at 25 °C and 40% respectively.

1.1 Characterization of electrospun scaffold

The morphology and microstructure of the scaffolds were observed by scanning electron microscopy (Hitachi SU5000, Hitachi, Japan) available at the electron microscopy facility of the ETH Zurich (ScopeM). One sample per condition (so, in total 12 samples) were analysed and they were glued onto SEM in stubs with a diameter of 20mm using a conductive carbon adhesive sticker. Prior to examination, each sample was coated with a 4nm thick Platinum-Palladium layer using a sputter coater (CCU-010, Safematic). The scaffolds were analysed before and after the mechanical tests.

1.2 Quasi-static uniaxial tensile mechanical tests of electrospun membranes

Before starting to characterize the fissure initiation and propagation properties of animal cartilage tissue samples and synthetic fibrous membranes, a tensile testing method was used to measure the base mechanical properties of engineered cartilage tissue scaffolds first and to develop a reliable and reproducible protocol. Scaffolds were prepared for mechanical tensile testing by following the ASTM F3510-21 standard for fiber-based constructs for tissue-engineered medical products. Electrospun specimens were prepared by first performing two plane parallel cuts through the scaffold with a microtome blade cutting jig, followed by die cutting the specimens into rectangles (4 cm x 1 cm) for testing. The rectangular sample shape used may be more appropriate for polymers and potentially reduces the edge effects as suggested in the ASTM F3510-21. The thickness of the specimens was determined with a profilometer (3D Optical Profilometer, Sensofar, Spain), to avoid modifying the polymer structure, as would be the case with SEM preparation. A uniaxial tensile test loading was performed by elongating the scaffolds, both along the fiber direction and in a random orientation. For this purpose, dehydrated specimens were held in custom-made clamps with a rough surface (to avoid slippage and deformation of the samples) on an Instron ElectroDynamic testing machine (ElectroPlus™ E10000 Dynamic Test Instrument, Instron, USA). The lower clamp was directly fixed on a 50 N force transducer (KD24s, Transmetra, Switzerland) and the top clamp was mounted to the moving actuator, as shown in Figure 2. As a back-up, a 1 kN load cell (bi-axial dynacell (1 kN / 25 Nm), Instron, USA) was used, onto which the 50 N force transducer was mounted. For each of the four structure types three independent samples were tested by performing a uniaxial tensile test under quasi-static conditions (0.1 mm/s) to determine modulus and tensile strength. The actual test was controlled by Instron's WaveMatrix™ software. The distance between the clamps was set to 20mm. A preload of 0.05N was applied before stretching the sample by 30 mm with a speed of 0.1 mm/s. This resulted in a theoretical strain of 150% for the region of interest in the middle of the samples.

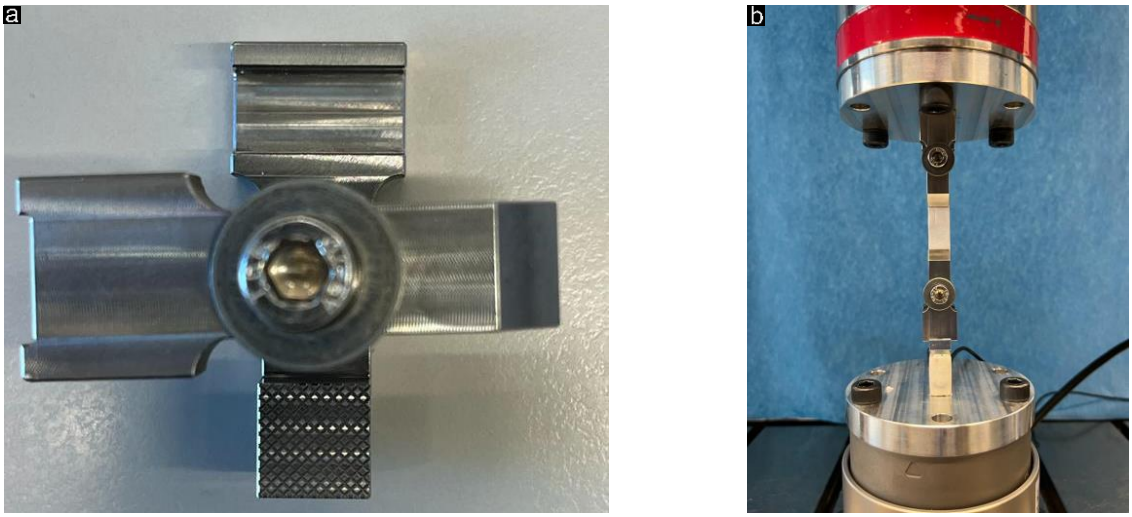

Figure 2: a) Photograph of the custom-made clamp. b) Photograph taken prior to starting a uniaxial tensile test.

More information about the actual state of deformation in the region of interest can be retrieved by optical methods for displacement and strain analysis. For soft materials tested at large strains in particular, Digital Image Correlation (DIC) has become an important tool. Therefore, future mechanical tests will be performed with the use of Digital Image Correlation (Isi-sys GmbH, Germany). The DIC uses full-field and non-invasive measurements, allowing the detection of displacements and deformations over the entire surface of the articular cartilage samples. Up until now, only the DIC camera system (Manta G-917B ASG, Allied Vision, Germany) was used and synchronized with the test sequence to take high-resolution pictures of the tests. An image was taken every 100 ms during the test. The actuator speed was set to 0.1 mm/s and moved up to 30 mm relative to the starting point.

1.3 Tensile crack propagation mechanical tests of electrospun membranes

To study the crack initiation and propagation properties and to have a direct comparison between the intact and damaged engineered scaffolds, a notch was induced on the same type of specimens. Prior to conducting the tensile loading test, a 2.27 mm notch was cut using a scalpel blade into the middle of the engineered cartilage samples respectively [23]. Tensile testing using notched specimens were performed as tensile stresses could be related to at least one mode of failure (fibrillation) in cartilage [23]. The analysis was carried out with the same procedure as described above (Figure 3) and the evolution of damage as a result of applied load was evaluated via DIC camera system (Manta G-917B ASG, Allied Vision, Germany). After the tests, short pieces of the cracked area were cut from the test samples and analysed via scanning electron microscopy (Hitachi SU5000, Hitachi, Japan).

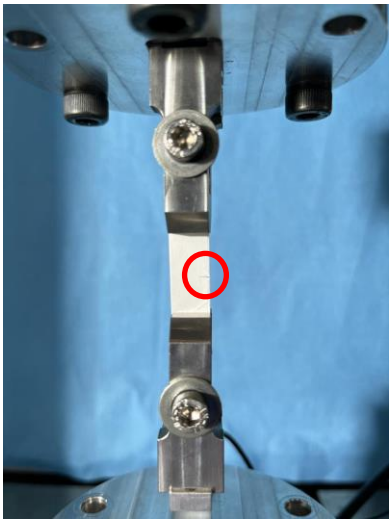

Figure 3: Photograph taken prior to starting a crack propagation tensile test with a notched sample.

1.4 Development of poro-viscoelastic FE models of fiber-reinforced cartilage and scaffold

Building on the work developed in our lab [24] [25], a three-dimensional biphasic fiber-reinforced cartilage model was extended. A poro-viscoelastic media was constrained to embedded hyperelastic fibers that follow the physiologically observed patterns of Benninghoff arcades. The shape and distribution of these fibers were mathematically formulated and produced using a Matlab routine. The user-defined hyperelastic material model was implemented using a FORTRAN subroutine. The model was analyzed using the commercial finite element software ABAQUS. The materials constants for both the matrix and the fibers were taken from the literature [24]. With the development of this model, we could first verify whether a generic cartilage model simulation can capture the experimental behavior of our membranes and thus also understand whether the membranes we are fabricating can exhibit typical cartilage characteristics. Then, following the continuum damage mechanics

model [26], we will simulate the damage in the model in order to characterize the properties of crack initiation and propagation. Finally, an improved FE model with experimental data will be implemented into a tissue-scale simulation model of fiber damage in fibrous tissues to better understand mechanical conditions which may cause cartilage damage.

2. Data Analysis

All the collected data was analysed in Jupiter notebooks, using Python 3.7.0. All graphs were obtained with Python (3.7.0) and GraphPad Prism (v3.2.0).

The following sample groups were compared:

Table 1: Comparison between sample groups

Comparison	***Sample Conditions***	***Number of samples***
Notched	Al_4h	3
Notched	Al_6h	3
Notched	Al_8h	3
Notched	Random	3
Intact	Al_4h	3
Intact	Al_6h	3
Intact	Al_8h	3
Intact	Random	3

Every tested structure was analyzed to determine the Young's modulus and ultimate strength. A virtual pre-load of 0.05 N was applied, meaning that only data points with a force greater than 0.05 N were included in the data analysis in order to compensate for any compression of the samples at the beginning of the tests. Apparent stress was computed from the displacement data of the actuator, and the initial distance between the clamps was 20 mm for all specimens. A simplified cross-sectional area (CSA) was used to compute the (engineering) stress, calculated as:

$$CSA = Height * Width$$

The structure height needed for the cross-sectional area, as previously discussed, was determined individually for every sample from each group with a profilometer (3D Optical Profilometer, Sensofar, Spain) and with the use of the Gwyddion software.

At this stage of the work, no statistical analysis was carried out as too few specimens were considered for each type of structure. Further analyses are ongoing to obtain a larger total number of samples.

3. Results

3.1 Characterization of electrospun scaffold

Scanning electron microscopy was used to analyze the membranes regarding overall morphology of the membranes and the fiber orientation obtained at different conditions. Figure 4 shows qualitatively how the combination of high rotational speed and conduction gaps might lead to a higher alignment of the fibers.

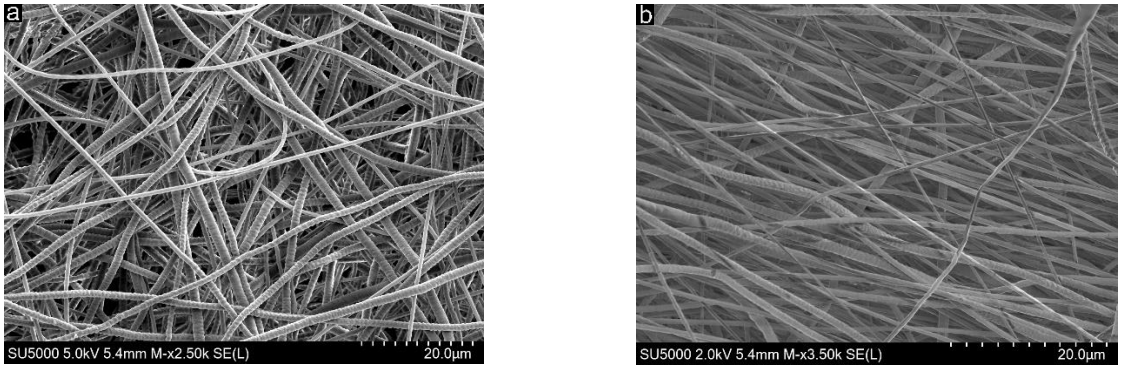

Figure 4: Scanning electron morphology pictures. a) Random fiber orientation b) Aligned fiber orientation

3.2 Quasi-static uniaxial tensile mechanical tests of electrospun membranes

For each structure type, three independent specimens (n = 3) were subjected to uniaxial tensile loads. Figure 5 depicts some frames of the loading history for the different sample conditions. From top to bottom respectively: random fiber orientation sample, notched random fiber orientation sample, aligned fiber orientation sample, notched aligned fiber orientation samples.

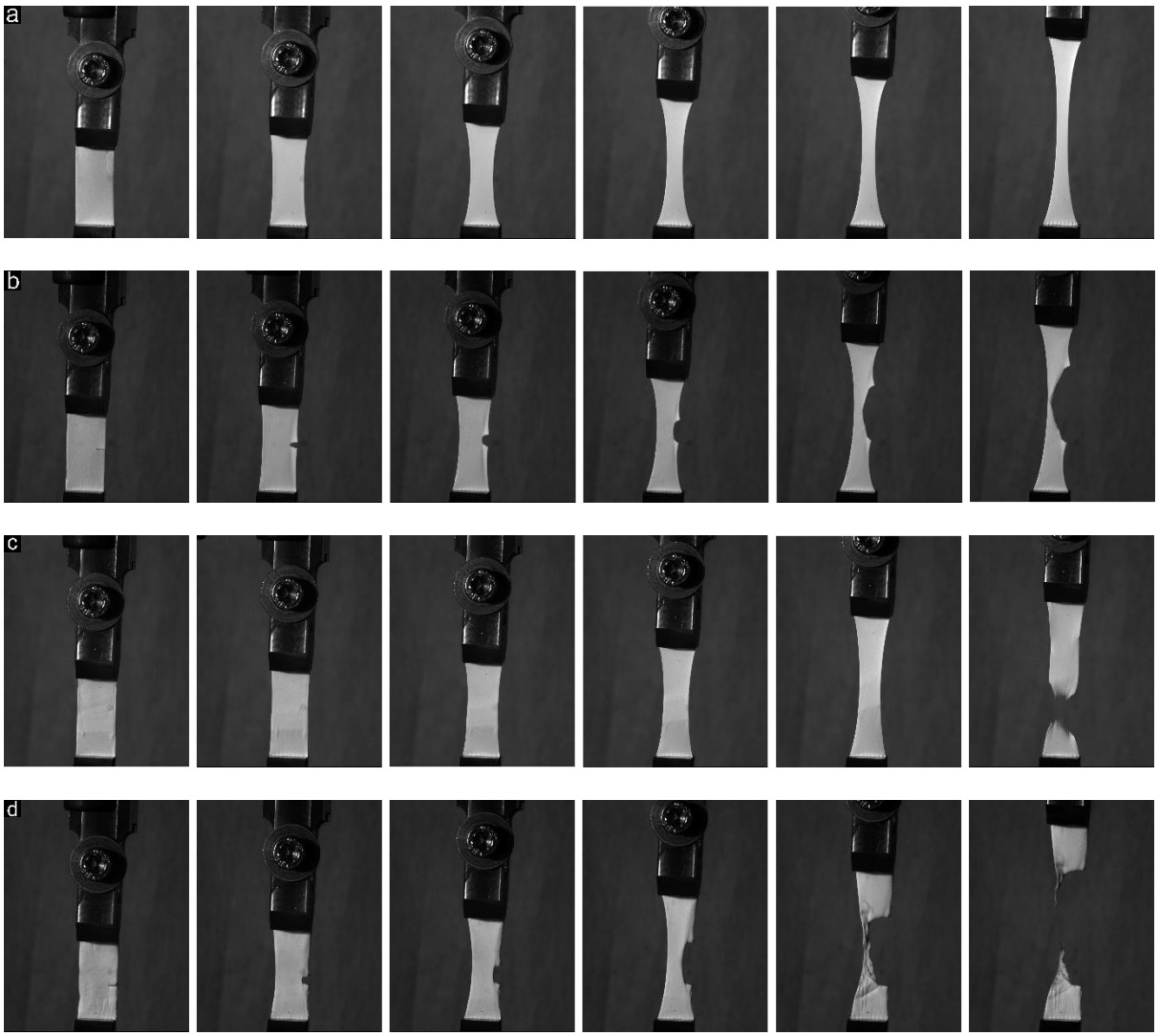

Figure 5: a) Optical images of electrospun samples with random fiber orientation. b) Optical images of notched electrospun samples with fiber orientation.c) Optical images of electrospun samples with aligned fiber orientation. d) Optical images of notched electrospun samples with aligned fiber orientation.

Visually, one can see that at the same time frame the Poisson's ratio seems to be much lower for the samples with the fibers aligned, providing a stiffer response. That is related to the fiber recruitment during test. From these pictures, it is also possible to see the shape of the notch propagation throughout the loading cycle. What can be observed is that the crack, instead of propagating, blurs to the breaking point.

Additionally, structure analysis was performed using the scanning electron microscope to evaluate the notch structure. In both sets of samples (with random and aligned fibers), it is possible to see the mark left by the scalpel. In the case of aligned fibers, the fibers remain aligned perpendicular to the cut line (Figure 6a – 6b). In Figure 6c it can be observed that for samples with aligned fibers, moving towards the breaking point, the alignment of the fibers changes and follows the notch conformation during stretching, and then some fibers start to pull out.

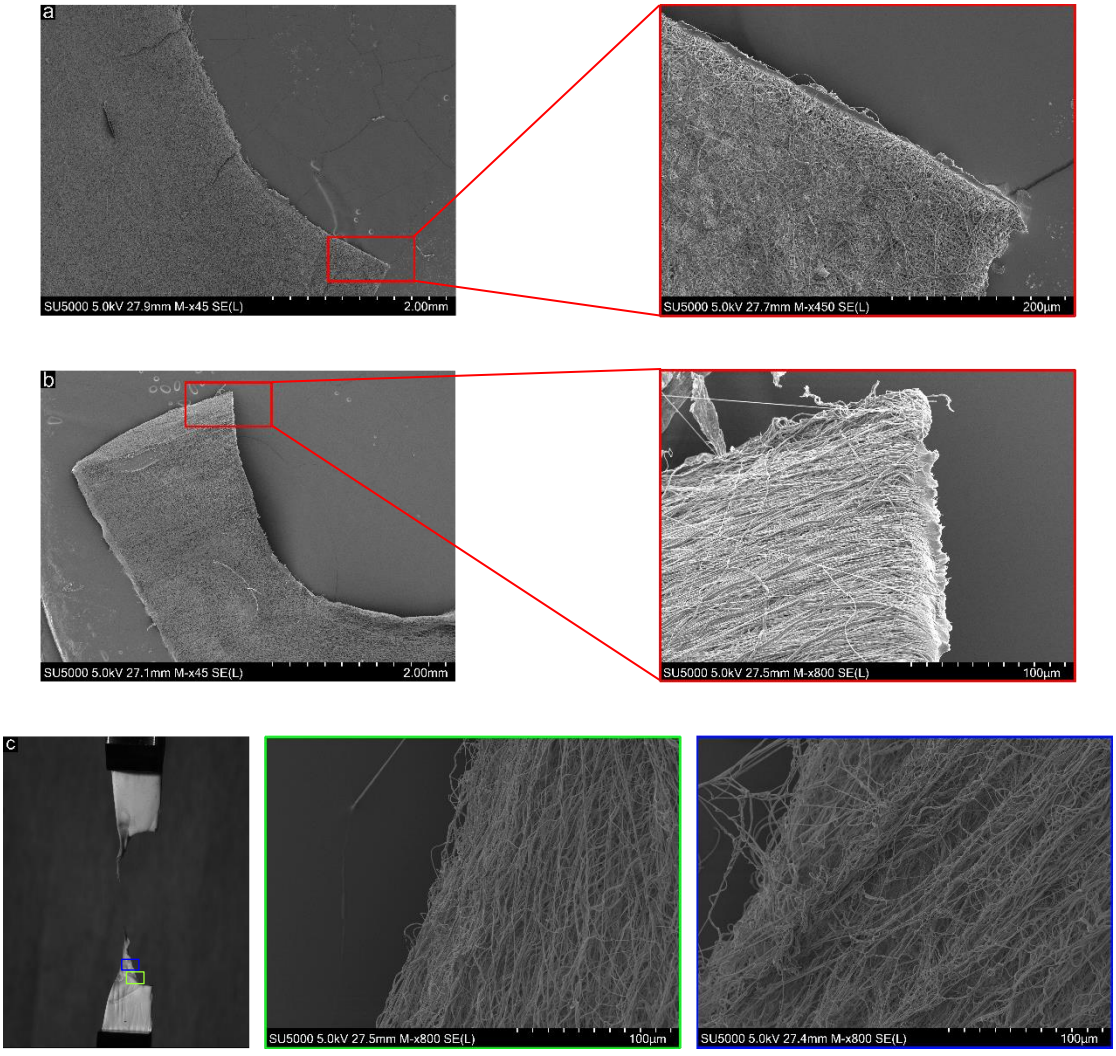

Figure 6: Scanning electron pictures of a) random fiber orientation and b) aligned fiber orientation samples. c) Scanning electron pictures of fibers orientation moving towards the breaking point of the sample.

Figure 7 depicts all obtained stress-strain curves. The different colour shades indicate the different sample conditions. A strain value of 1.0 is equal to 100% strain. Every structure type was tested with n = 3 samples. The difference between the curves with aligned and random fiber orientation samples is evident.

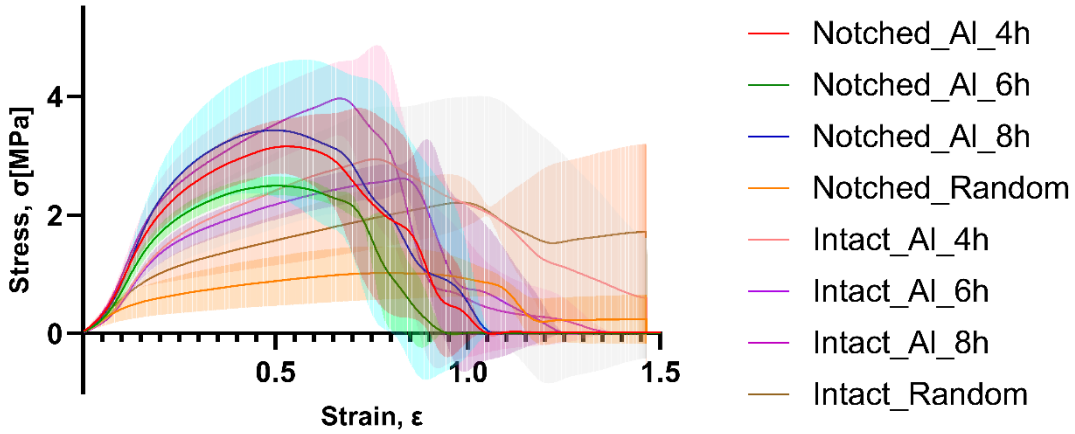

Figure 7: Line plot with Error Bars of stress-strain curves of all tested samples obtained from the uniaxial tensile test (n=3 per sample type)

In Figure 8, the Young's modulus for the different sample conditions is shown (for both intact and notched aligned electrospun membranes manufactured using different spinning times, as well intact and notched random electrospun membranes spun for 4h as comparison). The corresponding values are depicted in Table 2. While aligning fibres clearly increased the tensile E-moduli, the spinning times did not influence the tensile E-modulus. This however was expected, as the tensile modulus is scaled by the sample thickness.

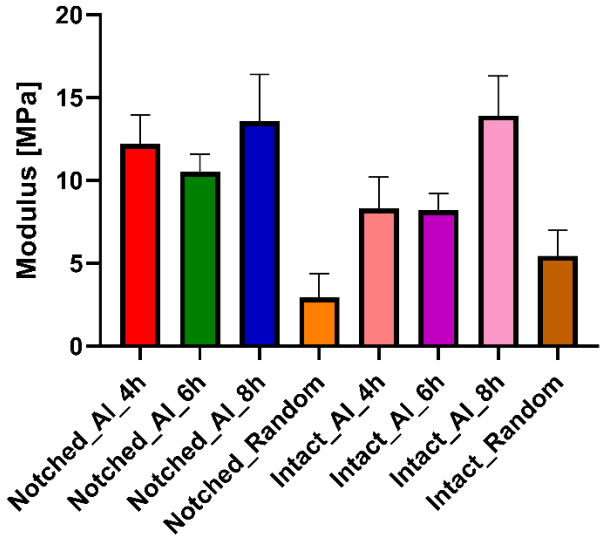

Figure 8: Young's moduli of all tested samples; colors indicate sample conditions.

Table 2: Means and standard deviations of Young's modulus for all sample conditions

Sample condition	***Mean ± SD [MPa]***
Notched_Al_4h	12.20 ± 1.74
Notched_Al_6h	10.53 ± 1.05
Notched_Al_8h	13.57 ± 2.81
Notched_Random	2.95 ± 1.43
Intact_Al_4h	8.30 ± 1.89
Intact_Al_6h	8.21 ± 1.02
Intact_Al_8h	13.92 ± 2.38
Intact_Random	5.44 ± 1.53

Figure 9 shows the ultimate stresses for all different conditions. The highest stresses were observed in the aligned fiber orientation samples with a 8hr-spin time. Table 3 depicts the corresponding values.

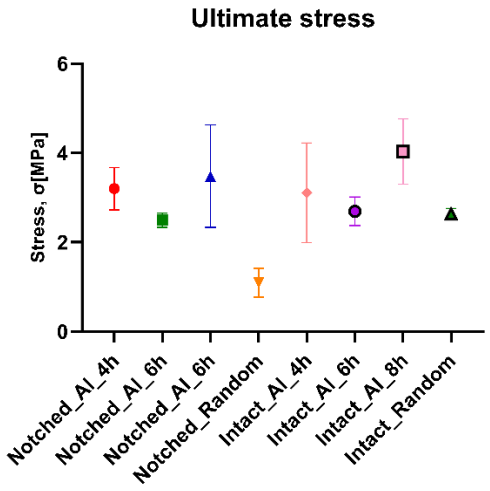

Figure 9: Ultimate stresses of all tested samples; colors indicate sample conditions

Table 3: Means and standard deviations of ultimate strength for all sample conditions

Sample condition	***Mean ± SD [MPa]***
Notched_Al_4h	3.02 ± 0.47
Notched_Al_6h	2.50 ± 0.16
Notched_Al_8h	3.48 ± 1.15
Notched_Random	1.10 ± 0.32
Intact_Al_4h	3.11 ± 1.11
Intact_Al_6h	2.70 ± 0.32
Intact_Al_8h	4.03 ± 0.73
Intact_Random	2.63 ± 0.12

3.3 Fiber-reinforced model for articular cartilage

Starting from the previous FE model discussed above [24], a first step has been to change the shape of the matrix that embeds the fibres from a cylindrical shape to a rectangular parallelepiped. Material properties were linear elastic with constants taken from the literature. The matrix was meshed with linear hexahedral elements (C3D8R) with reduced integration. The fibers were considered hyperelastic and the material properties were formulated in ABAQUS with a UMAT subroutine. The fibers, after adapting the Matlab code for the new rectangular shape of the matrix, were embedded as truss elements (T3D2) in the matrix using the embedded element technique available in ABAQUS. A first simulation to replicate the experimental tensile tests was run. Further analysis, improvements and a first validation with data experiments and other previously run FE models will follow.

4. Discussion

The combination of the isolating tape and the higher rotational speed allows to produce samples with a high degree of alignment. This higher directionality was qualitatively shown with SEM pictures. This is likely why a higher modulus was observed in membranes with an aligned fiber orientation compared to the random fiber orientation. This highlighted how fiber orientation strongly affects the tensile properties of the resulting electrospun scaffolds. Therefore, this could be advantageous for implanted conditions. To further assess the

fibre orientation, a quantitative analysis of fibre alignment is planned in the future based on SEM images and using ImageJ software (V. 1.51).

Regarding the production of the membranes, it could be observed from the tests that although the samples with the aligned fibers showed better behaviour in tension than those with the random fibers, these membranes always broke at the areas where the conductive gap tape had not been placed. A first improvement could therefore be the extension of the zone with the conductive gaps to a larger area of the sample.

The different spinning times used for the aligned membranes were intended to replicate the same thickness as the random membranes, which were considered our benchmark. The deposition of aligned fibres using conductive gaps is less efficient compared to randomly deposited fibres. Therefore, it was only essential to evaluate membrane thickness as a function of spinning time for the membranes consisting of aligned fibres.
As it has been shown that different spinning times yield different membrane thickness, it is planned to further investigate thickness vs. spinning time as a necessary part of scaling up the process and expanding its application.

Furthermore, melt electrowriting (MEW) has been recently established as an alternative fabrication method to electrospinning and fused deposition modeling (FDM, 3D-printing) [27]. In contrast to solvent electrospinning, which uses an applied electric field to accelerate and extend the polymer fiber, melt electrowriting requires the extrusion of a molten thermoplastic. As the next step in this work, a multi-scale approach structure purely based on melt electrowriting will be considered based on generating fibers with diameters below the µm range. While electrospinning requires a polymer to be brought to the liquid state using an appropriate solvent, MEW uses polymer in its molten state without the need for any liquefier. Furthermore, MEW allows for the precise deposition of the produced fiber. In contrast, electrospinning is a relatively random process [15].
MEW enables the development of highly porous (80-98% pore volume), sophisticated and biomimetic scaffolds. The idea is that a MEW network could direct cartilage-specific tissue organization while also supporting the resulting hybrid construct in a way similar to the collagen network in articular cartilage. In that way, it could specifically provide tensile strength and stiffness but make little contribution to the tissue's compressive properties without proteoglycans [12]. MEW has the potential to advance TE applications because of 1) improved resolution, 2) the ability to fabricate large volume scaffolds and 3) the ability to integrate multi-modal diameters into a single fabrication step [27].

A first attempt has been made. For the microfiber mesh, 20 layers of 250 µm spaced grid mesh have been melt electrowritten. For the nanofiber mesh, 10 layers x 12 different types of orientation (0°, 15°, 30°,…,165°) will be melt electrowritten. For microfibers measurements, 10 random fibers were selected and measured manually for each sample (n=3). The nanofiber diameters for 3 samples were measured using the DiameterJ plugin in the ImageJ software. In a pilot study, it has been shown that nanofibers are obtainable using MEW. The fiber diameter obtained from the microfiber grid was found to be 19.141 ± 0.424 µm. On the other hand, fiber diameters from the nanofiber mesh were found to be 0.694 ± 0.029 µm (Figure 10d). MEW allows for superior control of fiber orientation of the mesh, compared to electrospinning. Furthermore, MEW does not require the usage of solvents as in contrast to electrospinning. The usage of solvents in electrospinning might render the nanofibers toxic to cells.

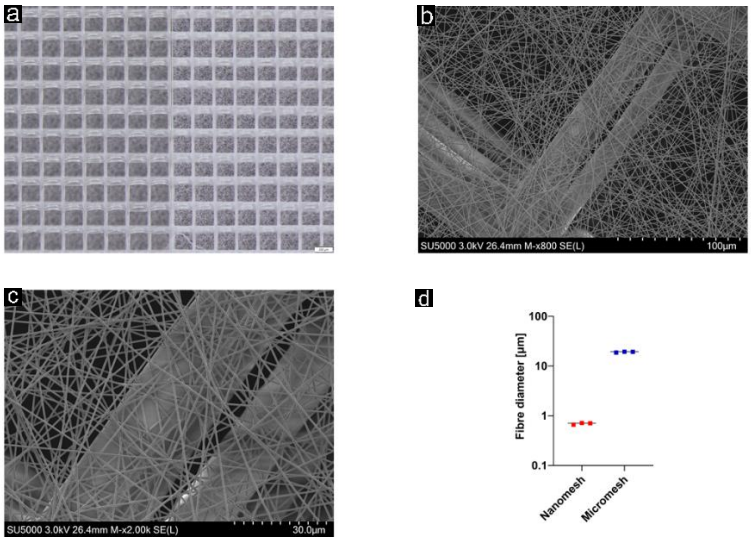

Figure 10: a) Stereo microscope (Olympus SZX16, Olympus, Japan) image of the overview of the structure. The micromesh structure is on the left side of the image, while the nanomesh structure is on the right side of the image. b) SEM (Hitachi SU5000, Hitachi, Japan) image of the hierarchical nano- and microfibrous tissue scaffold with a magnification of 800x. c) SEM (Hitachi SU5000, Hitachi, Japan) image of the hierarchical nano- and microfibrous tissue scaffold with a magnification of 2000x. It is possible to see nicely the comparison between the 2 different fibers dimensions d) Fiber diameter distributions for nanomesh and micromesh structures.

From the notch propagation results, in section 3.2, the notch blunted instead of propagating. This is not surprising, since it is a distinguishing feature of fracture behaviour in soft materials. It is interesting to see how with high-resolution cameras such as those used in these experiments, we are able to keep track of the shape and mode of notch propagation. Therefore, both the uniaxial tensile loading tests with intact and notched samples and the dynamic cyclic loading test will soon be performed with the use of the Digital Image Correlation (DIC). Using these tools, the deformation and microstructure around the crack tip for notched samples before and after loading could be characterized.

As a further mechanical analysis, in order to examine fibre network integrity, material creep, and hysteresis of these artificial membranes, dynamic cyclic loading tests will be performed at 1 Hz, between 0 – 50% yield strain. For this testing, at least 5 independent scaffolds will be prepared for each set of electrospun specimens from each orientation. The same applies for each set of melt electrowritten samples.

As a representative comparison, the same type of notch and analysis will soon be carried out on bovine articular cartilage samples in parallel. The bovine cartilage specimens from the knee joint will be obtained from a local slaughterhouse. A 30 mm x 10 mm rectangular sample block consisting of cartilage will be extracted from the interpatellar groove, medial and lateral condyles of each femur, and the respective counterpart of the tibia. The samples will be sliced to the desired thickness with the use of a Vibratome (Leica VT1200/S, Leica, Germany) available at the histology facility of the ETH Zürich (ScopeM). To the best of knowledge of the author, only a few studies have been published about similar tests on bovine articular cartilage [23] [19], and none of them on mechanical properties of cracked engineered articular cartilage under uniaxial tensile and cyclic tensile loading. We expect the fiber orientation to strongly affect the tensile properties. This will underline how fiber orientation is a key factor in dictating the evolution of surface damage on the surface. To further improved the reliability and reproducibility of these tests, a custom-made sample holder will be designed to avoid misalignment of the samples.

The same protocol will be performed on a more reliable experimental condition in collaboration with Luleå Technical University (LTU). At LTU, the test will be carried out in a temperature-controlled bovine serum or synovial fluid bath a 37°C and with a 3-point bending mode Instron.

About the FE model, in conjunction with Imperial College London (ICL), this approach will be compared with a fiber-reinforced poroelastic model of fiber-reinforced matrices. The model will be based on previous work from Dr. Rob Hewson's group and colleagues at ICL. Complimentary training on computational modeling of fracture mechanics will be carried out; methods and approaches of the ICL will be used to optimize the model to simulate the failure mechanism.

Summary

In this report, we highlighted how electrospinning represents a valid method to produce stochastic or aligned porous fibrous materials that mimic soft tissue's natural collagenous extracellular matrix. Furthermore, we introduced a testing method to determine the tensile mechanical properties of electrospun membranes, both for intact and damaged scaffolds. Up to now, since tensile stresses are the main form of notch opening and the most frequently used for cartilage, we focused on this mode of fracture loading. This protocol is very efficient and reliable for evaluating the fracture mechanism in fibrous membranes under the tensile loading mode. This method, together with the FE model, and other type of mechanical tests, will be applied in the future project tasks to obtain the further insight into the mechanical properties of fissure initiation and propagation of multiscale fibrous membranes. These will help to identify articulating conditions that may cause damage.

References

1. HunterDJ, B., *ZeinstraS. Osteoarthritis.* Lancet, 1759. **393**(10182): p. 1745.
2. Chen, D., et al., *Osteoarthritis: toward a comprehensive understanding of pathological mechanism.* Bone research, 2017. **5**(1): p. 1-13.
3. Griffin, T.M. and F. Guilak, *The role of mechanical loading in the onset and progression of osteoarthritis.* Exercise and sport sciences reviews, 2005. **33**(4): p. 195-200.
4. Egloff, C., T. Hügle, and V. Valderrabano, *Biomechanics and pathomechanisms of osteoarthritis.* Swiss medical weekly, 2012(29).
5. Leifer, V., J. Katz, and E. Losina, *The burden of OA-health services and economics.* Osteoarthritis and Cartilage, 2022. **30**(1): p. 10-16.
6. Jonsson, H., et al., *Incidence and prevalence of total joint replacements due to osteoarthritis in the elderly: risk factors and factors associated with late life prevalence in the AGES-Reykjavik Study.* BMC musculoskeletal disorders, 2016. **17**(1): p. 1-8.
7. Elahi, S.A., et al., *An in silico framework of cartilage degeneration that integrates fibril reorientation and degradation along with altered hydration and fixed charge density loss.* Frontiers in bioengineering and biotechnology, 2021. **9**: p. 529.
8. Slater, G. and T. Slater, *Articular Cartilage-A Literature Review.* J Regen Biol Med, 2022. **4**(1): p. 1-10.
9. Elliott, M. and G. Slater, *Journal of Regenerative Biology and Medicine.* 2019.
10. Hodgkinson, T., et al., *Mechanosignalling in cartilage: an emerging target for the treatment of osteoarthritis.* Nature Reviews Rheumatology, 2022. **18**(2): p. 67-84.
11. Xiao, Y., et al., *Mechanical testing of hydrogels in cartilage tissue engineering: beyond the compressive modulus.* Tissue Engineering Part B: Reviews, 2013. **19**(5): p. 403-412.
12. Dufour, A., et al., *Integrating melt electrowriting and inkjet bioprinting for engineering structurally organized articular cartilage.* Biomaterials, 2022. **283**: p. 121405.
13. Accardi, M.A., et al., *Effects of fiber orientation on the frictional properties and damage of regenerative articular cartilage surfaces.* Tissue Engineering Part A, 2013. **19**(19-20): p. 2300-2310.
14. Alexeev, D., et al., *Mechanical evaluation of electrospun poly (ε-caprolactone) single fibers.* Materials Today Communications, 2020. **24**: p. 101211.

15. Alexeev, D., et al., *Electrospun biodegradable poly (ε-caprolactone) membranes for annulus fibrosus repair: Long-term material stability and mechanical competence.* JOR spine, 2021. **4**(1): p. e1130.
16. Patel, J.M., et al., *A systematic review and guide to mechanical testing for articular cartilage tissue engineering.* Tissue Engineering Part C: Methods, 2019. **25**(10): p. 593-608.
17. Ding, C., et al., *Knee cartilage defects: association with early radiographic osteoarthritis, decreased cartilage volume, increased joint surface area and type II collagen breakdown.* Osteoarthritis and cartilage, 2005. **13**(3): p. 198-205.
18. Bircher, K., et al., *Tear resistance of soft collagenous tissues.* Nature communications, 2019. **10**(1): p. 1-13.
19. Si, Y., et al., *Mechanical properties of cracked articular cartilage under uniaxial creep and cyclic tensile loading.* Journal of Biomechanics, 2022. **134**: p. 110988.
20. Julkunen, P., et al., *A review of the combination of experimental measurements and fibril-reinforced modeling for investigation of articular cartilage and chondrocyte response to loading.* Computational and mathematical methods in medicine, 2013. **2013**.
21. Mäkelä, J.T., M.R. Huttu, and R.K. Korhonen, *Structure–function relationships in osteoarthritic human hip joint articular cartilage.* Osteoarthritis and cartilage, 2012. **20**(11): p. 1268-1277.
22. Bissacco, E., et al., *Effect of Conduction Gaps and Increased Collector Rotation Speed on Electrospun PCL Matrices.*
23. McCormack, T. and J.M. Mansour, *Reduction in tensile strength of cartilage precedes surface damage under repeated compressive loading in vitro.* Journal of biomechanics, 1997. **31**(1): p. 55-61.
24. Christen, P., P.D.S. Ferguson, and S. Chegini, *Master of Science in Biomedical Engineering Thesis Contact Mechanics of a Discrete Fiber-Reinforced Cartilage Model.* 2009.
25. Chegini, S., *Constituent-based Tissue Models for the Simulation of Hip Joint Pathologies*. 2009, Verlag nicht ermittelbar.
26. Voyiadjis, G.Z. and P.I. Kattan, *Damage mechanics*. 2005: CRC Press.
27. Dalton, P.D., *Melt electrowriting with additive manufacturing principles.* Current Opinion in Biomedical Engineering, 2017. **2**: p. 49-57.